ACS APPLIED MATERIALS & INTERFACES

Research Article

www.acsami.org

Eu^{2+}-Activated $Sr_8ZnSc(PO_4)_7$: A Novel Near-Ultraviolet Converting Yellow-Emitting Phosphor for White Light-Emitting Diodes

Chien-Hao Huang,*[,†] Yi-Chen Chiu,[†] Yao-Tsung Yeh,[†] Ting-Shan Chan,[‡] and Teng-Ming Chen*[,§]

[†]Material and Chemical Research Laboratories, Industrial Technology Research Institute, Hsinchu, Taiwan 30011, Republic of China

[‡]National Synchrotron Radiation Research Center, Hsinchu Science Park, Hsinchu, Taiwan 30076, Republic of China

[§]Phosphors Research Laboratory and Department of Applied Chemistry, National Chiao Tung University, Hsinchu, Taiwan 30010, Republic of China

Supporting Information

ABSTRACT: The crystal structure of Eu^{2+}-activated $Sr_8ZnSc(PO_4)_7$:Eu^{2+} phosphor was refined and determined from XRD profiles by the Rietveld refinement method using a synchrotron light source. This phosphor crystallizes in the monoclinic structure with the $I2/a$ space group. The SZSP:xEu^{2+} phosphors showed a broad yellow emission band centered at 511 and 571 nm depending on the concentration of Eu^{2+}, and the composition-optimized concentration of Eu^{2+} in the $Sr_8ZnSc(PO_4)_7$:Eu^{2+} phosphor was determined to be 2 mol %. The estimated crystal-field splitting and CIE chromaticity coordinates of $Sr_8ZnSc(PO_4)_7$:xEu^{2+} (x = 0.001−0.05 mol) were 20181−20983 cm^{-1} and (0.3835, 0.5074) to (0.4221, 0.5012), respectively, and the emission band showed a redshift from 547 to 571 nm with increasing Eu^{2+} concentration. The nonradiative transitions between the Eu^{2+} ions in the $Sr_8ZnSc(PO_4)_7$ host were attributable to dipole−dipole interactions, and the critical distance was approximately 19.8 Å. The combination of a 400 nm NUV chip with a blend of $Sr_8ZnSc(PO_4)_7$:0.02Eu^{2+} and BAM:Eu^{2+} phosphors (light converters) gave high color rendering indices between 79.38 and 92.88, correlated color temperatures between 4325 and 7937 K, and tuned CIE chromaticity coordinates in the range (0.381, 0.435) to (0.294, 0.310), respectively, depending on the SZSP:0.02Eu^{2+}/BAM:Eu^{2+} weight ratio. These results suggest that the $Sr_8ZnSc(PO_4)_7$:0.02Eu^{2+}/BAM:Eu^{2+} phosphor blend has potential applications in white NUV LEDs.

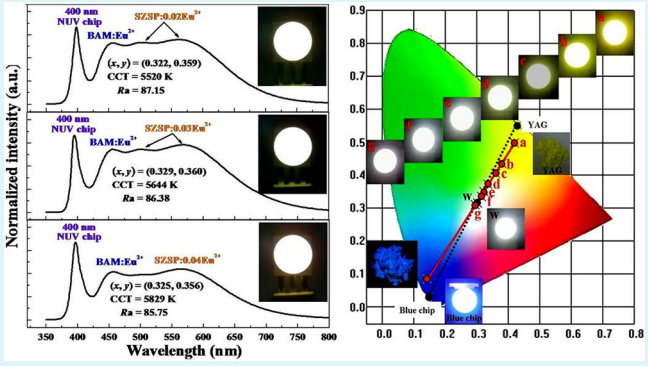

KEYWORDS: *$Sr_8ZnSc(PO_4)_7$, yellow-emitting, Eu^{2+}, NUV, white LED, photoluminescence*

1. INTRODUCTION

In 1996, Nichia coupled their blue LED with the yellow-emitting $Y_3Al_5O_{12}$:Ce^{3+} (YAG:Ce^{3+}) and developed white LEDs. Thereafter, much effort has been focused on white LEDs, both in academia and in the industry worldwide. In recent years, white LEDs have attracted much attention because of their high efficiency, small size, compactness, safety (these LEDs are mercury-free), high material stability, long operational lifetime, and resultant energy-saving capacity. Hence, these LEDs are expected to replace conventional incandescent and fluorescent lamps for general lighting applications in the near future.[1−3] An LED, however, generates only a limited amount of light and single color at a time. To obtain white light for solid-state lighting, emission spanning the visible spectrum (red, green, and blue) must be generated in the appropriate proportions. To achieve this effect, researchers generally used three approaches for generating white light with LEDs: (a) combining with trichromatic RGB LED chip;[4] (b) blue-light LED chip comprised of yellow-emitting phosphor of YAG:Ce^{3+};[5] (c) ultraviolet/near-ultraviolet (UV/NUV) chip pumped of a phosphor blend of RGB-emitting phosphors.[6,7] The disadvantage of trichromatic RGB LED systems is that individual colored LEDs respond differently to the drive current, dimming, operating temperature, and operating time; furthermore, the controls required for color consistency serve to increase the cost factor. The major disadvantages of the combination of a blue InGaN chip and a YAG:Ce^{3+} phosphor are the poor color rendering index (75), which results from the lack of red spectral contribution, and the high color temperature (7756 K).[8] Integration of RGB-emitting phosphors with a UV/NUV chip for white-emitting system does help in generating white light, but this approach is expensive, and the luminous efficiency may degrade because of reabsorption. Recently, white LEDs fabricated using NUV chips (380−420 nm) coupled with a blend of blue- and yellow-emitting phosphors have been found to show favorable

Received: August 30, 2012
Accepted: November 21, 2012
Published: November 21, 2012

properties, including tunable correlated color temperature (CCT), high color-rendering index (CRI, *Ra*), and tunable CIE chromaticity coordinates. Therefore, the development of new yellow-emitting phosphors that can be effectively excited in the NUV range is a very important prospect that requires prompt attention. Many yellow-emitting phosphors for NUV LEDs have been identified and investigated, for example, $Ba_2Gd(BO_3)_2Cl:Eu^{2+}$,[9] $Ba_2Mg(BO_3)_2:Eu^{2+}$,[10] $Ba_2Mg(PO_4)_2:Eu^{2+}$,[11] γ-$Ca_2SiO_4:Ce^{3+},Li^+$,[12] $Sr_3B_2O_6:Eu^{2+}$,[13] $Sr_3SiO_5:Ce^{3+},Li^+$,[14] and $Y_2(CN_2)_3:Ce^{3+}$.[15]

To the best of our knowledge, the crystal structures and luminescence properties of $Sr_8ZnSc(PO_4)_7:xEu^{2+}$ have not yet been reported. In this study, we focus on the preparation of a series of yellow-emitting $Sr_8ZnSc(PO_4)_7:Eu^{2+}$ phosphors and investigate their crystal structure, luminescence properties, and reflectance spectra. We have also successfully fabricated a white pc-LED by using a blend of yellow-emitting $Sr_8ZnSc(PO_4)_7:Eu^{2+}$ and blue-emitting $BaMgAl_{10}O_{17}:Eu^{2+}$ ($BAM:Eu^{2+}$) phosphors with a 400 nm NUV LED chip and examined its optical properties. The results indicate that the yellow-emitting $Sr_8ZnSc(PO_4)_7:Eu^{2+}$ phosphor has great potential for applications in white NUV LEDs.

2. EXPERIMENTAL SECTION

2.1. Materials and Synthesis. The polycrystalline phosphors composed of $Sr_8ZnScY(PO_4)_7:xEu^{2+}$ ($SZSP:xEu^{2+}$) were prepared by a solid-state reaction in which the constituent raw materials $SrCO_3$ (A. R., 99.9%), ZnO (A. R., 99.99%), Sc_2O_3 (A. R., 99.99%), $(NH_4)_2HPO_4$ (Merck ≥99%), and Eu_2O_3 (A. R., 99.99%) were weighed in stoichiometric proportions. The powder mixtures were sintered under a reducing atmosphere (15% H_2/85% N_2) at 1300 °C for 8 h with one intermittent regrinding to prevent the possibility of incomplete reaction.

2.2. Materials Characterization. The crystal structure for phase formation was refined and determined by using synchrotron XRD profiles with λ = 0.7749 Å, recorded with a large Debye−Scherrer camera installed at beamline 01C2 of National Synchrotron Radiation Research Center (NSRRC) in Hsinchu, Taiwan; the GSAS program[16] was used for the structural refinements. The photoluminescence (PL) and photoluminescence excitation (PLE) spectra of the samples were analyzed by using a Spex Fluorolog-3 Spectrofluorometer equipped with a 450-W Xe light source. The Commission International de I'Eclairage (CIE) chromaticity coordinates for all samples were measured by a Laiko DT-101 color analyzer equipped with a CCD detector (Laiko Co., Tokyo, Japan). Diffuse reflectance spectra of phosphor samples were measured with a Hitachi 3010 double-beam UV−visible (vis) spectrometer (Hitachi Co., Tokyo, Japan) equipped with a Ø60 mm integrating sphere whose inner face was coated with $BaSO_4$ or Spectralon, and α-Al_2O_3 was used as a standard in the measurements. Thermal quenching measurements were investigated using a heating apparatus (THMS-600) in combination with the PL equipment.

2.3. White-Light LED Lamps Fabrication. White LED lamps were fabricated by integrating a mixture of transparent silicone resin and phosphors blend of yellow-emitting $Sr_8ZnSc(PO_4)_7:xEu^{2+}$ (x = 0.01, 0.02, 0.03, 0.04) and blue-emitting $BaMgAl_{10}O_{17}:Eu^{2+}$ commodity on an 400 nm NUV chip (AOT Product No: C06HC, Spec: 400 V10C, wavelength peak: 395−400 ± 1.32 nm, chip size: 40 × 40 mil^2, VF1: 3.8−4.0 ± 0.06 V, IV1: 90−100 ± 2.65 mW) and roast at 120 °C/10 h afterward.

3. RESULTS AND DISCUSSION

3.1. Crystal Structure. Figure 1 shows the observed (crosses), calculated (solid line), and difference (bottom) synchrotron XRD profiles for the Rietveld refinement of $Sr_8ZnSc(PO_4)_7$ and $Sr_8ZnSc(PO_4)_7:0.05Eu^{2+}$ phosphors at

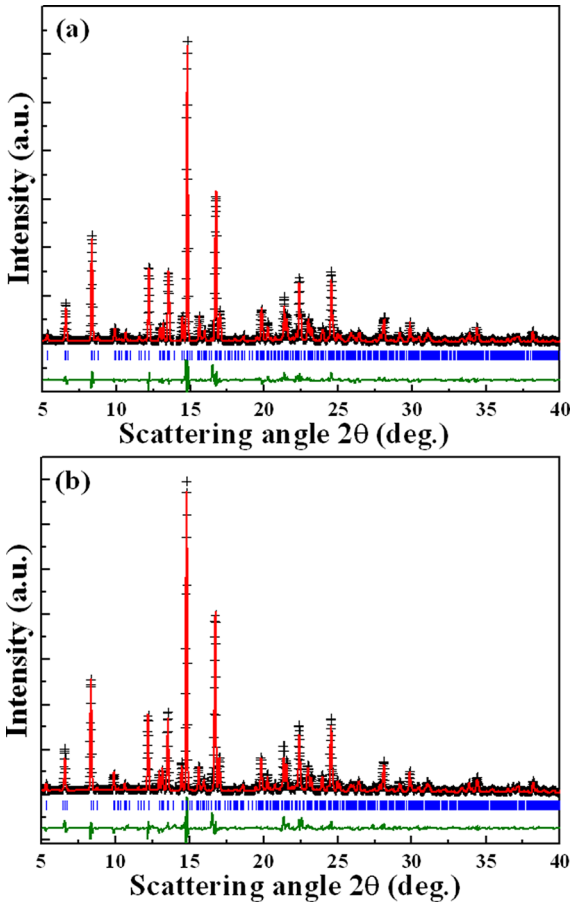

Figure 1. Observed (crosses), calculated (solid line), and difference (bottom) synchrotron XRD profiles for the Rietveld refinement of (a) $Sr_8ZnSc(PO_4)_7$; (b) $Sr_8ZnSc(PO_4)_7:0.05Eu^{2+}$ phosphors at 298 K with λ = 0.7749 Å. Bragg reflections are indicated by tick marks.

298K with λ = 0.7749 Å. The Rietveld refinement results indicate that neither the host nor the doped 0.05 mol Eu^{2+} ions caused any impurity or secondary phases in SZSP host structure. The $Sr_8ZnSc(PO_4)_7:xEu^{2+}$ crystallizes as a monoclinic structure with space group $I2/a$. For $Sr_8ZnSc(PO_4)_7$ crystal, the lattice parameters were determined to be a = 18.0681(9) Å, b = 10.6813(5) Å, c = 18.4116(9) Å, V = 2600.74(23) $Å^3$ and the refinement finally converged to R_p = 9.06%, R_{wp} = 13.05%, and χ^2 = 5.31. As Sr^{2+} was substituted by a small Eu^{2+} ion in $Sr_8ZnSc(PO_4)_7$ host, the lattice parameters of $Sr_8ZnSc(PO_4)_7:0.05Eu^{2+}$ became a = 18.0597(10) Å, b = 10.6744(6) Å, c = 18.4036(9) Å, V = 3510.8 $Å^3$, and the refinement finally converged to R_p = 9.49%, R_{wp} = 13.79%, and χ^2 = 5.81, which was shown in Table 1. All atom positions and occupancies factors for $Sr_8ZnSc(PO_4)_7:0.05Eu^{2+}$ phosphors were shown in Table S1 in the Supporting Information.

The simulation of the crystal structure of $Sr_8ZnSc(PO_4)_7$ using Rietveld refinement is shown in Figure 2. $Sr_8ZnSc(PO_4)_7$ is isostructural to β-$Ca_3(PO_4)_2$ crystal structure. In the β-$Ca_3(PO_4)_2$ crystal structure, the Ca^{2+} cations occupy five positions and one vacancy; Ca1 and Ca2 are eight-coordinated, Ca3 is nine-coordinated by oxygen atoms, the distorted octahedral (six-coordinated) Ca5 site is fully occupied, Ca4 is surrounded by nine oxygen atoms and half-occupied by calcium cations, and Ca6 is a vacancy. The Sr/Zn2, (Sr/Zn1, Sr/Zn3, Sr/Zn4, Sr/Zn5), Sr/Zn6, and Sc sites in the $Sr_8ZnSc(PO_4)_7$ structure[17] correspond to the (Ca1, Ca2), Ca3, (Ca4, Ca6),

dx.doi.org/10.1021/am302014e | ACS Appl. Mater. Interfaces 2012, 4, 6661−6668

Table 1. Rietveld Refinement and Crystal Data of $Sr_8ZnSc(PO_4)_7$ and $Sr_8ZnSc(PO_4)_7$:0.05Eu^{2+} Phosphors

formula	$Sr_8ZnSc(PO_4)_7$	$Sr_8ZnSc(PO_4)_7$:0.05Eu^{2+}
radiation type (Å)	0.7749	0.7749
2θ range (deg.)	5−40	5−40
T (K)	298	298
form wt	1476.18	1501.92
symmetry	monoclinic	monoclinic
space group	$I2/a$	$I2/a$
a (Å)	18.0681(9)	18.0597(10)
b (Å)	10.6813(5)	10.6744(6)
c (Å)	18.4016(9)	18.4136(9)
$\alpha = \gamma$ (deg)	90	90
β (deg)	132.9186(20)	132.9141(24)
V (Å^3)	2600.74(23)	2599.71(26)
Z	4	4
R_p (%)	9.06	9.49
R_{wp} (%)	13.05	13.79
χ^2	5.31	5.81

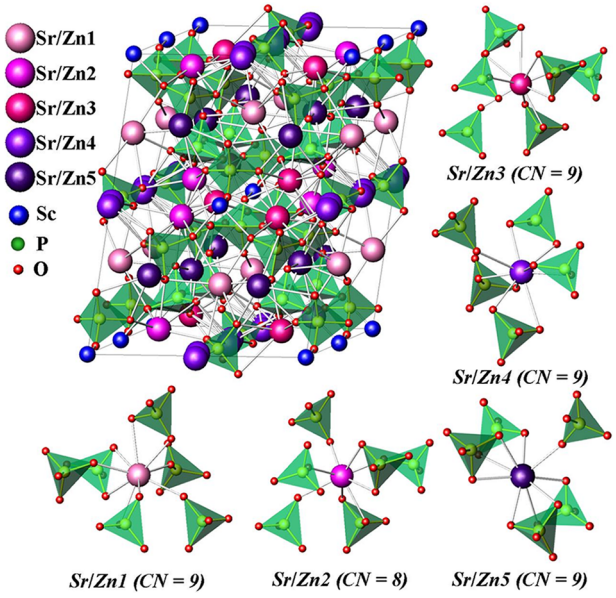

Figure 2. Crystal structure of $Sr_8ZnSc(PO_4)_7$.

and Ca5 sites in the β-$Ca_3(PO_4)_2$-type structure, respectively. In the $Sr_8ZnSc(PO_4)_7$ crystal structure, an 8*f* site corresponding to the Ca4 and Ca6 sites in the β-$Ca_3(PO_4)_2$-type structure is vacant and Sr/Zn has five different coordination numbers: Sr/Zn2 is defined to be eight-coordinated; Sr/Zn1, Sr/Zn3, Sr/Zn4, and Sr/Zn5 are nine-coordinated; Sc is six-coordinated; and P shows four four-coordination. The ionic radii for eight- and nine-coordinated Sr^{2+} are 1.26 and 1.31 Å, eight-coordinated Zn^{2+} is 0.9 Å, six-coordinated Sc^{3+} is 0.745 Å, respectively. However, the ionic radii for six-, eight- and nine-coordinated Eu^{2+} are 1.17, 1.25, and 1.3 Å. On the basis of ionic radii, the Eu^{2+} ions are expected to randomly occupy the Sr^{2+} or Zn^{2+} or Sc^{3+} ions sites in the SZSP host.

3.2. Photoluminescence Properties. Figure 3 illustrates the PL/PLE spectra of the $Sr_8ZnSc(PO_4)_7$:xEu^{2+} (x = 0.001−0.05 mol) phosphors under 400 nm excitation. Figure 3a shows the normalized PLE spectra of a series of SZSP:xEu^{2+} phosphors. The PLE spectrum shows a broad hump between 240 and 500 nm, which is attributed to the $4f^7 \rightarrow 4f^65d^1$

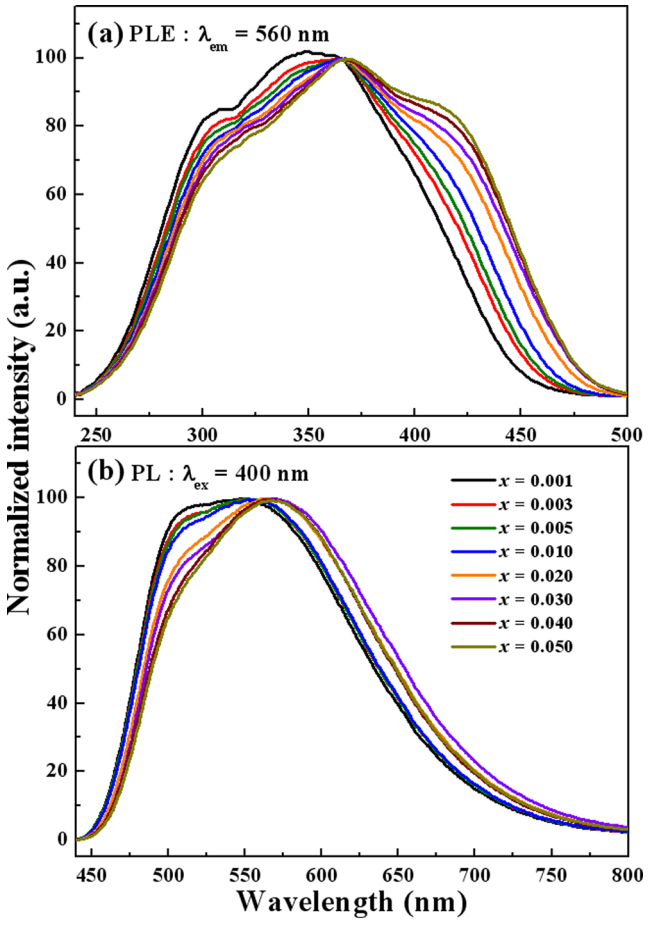

Figure 3. (a) Excitation and (b) emission spectra of $Sr_8ZnSc(PO_4)_7$:xEu^{2+} (x = 0.001−0.05 mol) phosphors under 400 nm excitation.

transition of the Eu^{2+} ions. The full width at half-maximum (FWHMs) of the SZSP:xEu^{2+} PLE spectra increases from 132 to 156 nm with increasing Eu^{2+} content, as shown in Table 2. The broad excitation band matches well with the range of the NUV LED chip (380−420 nm). Figure 3b shows the emission spectra of Eu^{2+} for different values of x (x = 0.001−0.05 mol) in SZSP:xEu^{2+} phosphors. The PL spectra of the SZSP:xEu^{2+} phosphors show broad yellow emission bands from 450 to 800 nm, which can be attributed to the $4f^65d^1 \rightarrow 4f^7$ transition of the Eu^{2+} ions.[18] When the doped concentration of Eu^{2+} is increased in SZSP:xEu^{2+} phosphors, the peak emission wavelength is red-shifted from 547 to 571 nm. The red-shift is mainly ascribed to the change in the crystal-field splitting of Eu^{2+}. The crystal-field splitting of Eu^{2+} (shown in Table 2) is estimated to be 20181−20983 cm^{-1} in $Sr_8ZnSc(PO_4)_7$ (x = 0.001−0.05 mol).[19] This phenomenon can be explained in terms of energy transfer from the Eu^{2+} ions at the higher 5d levels to those at the lower levels, which causes a decrease in the emission energy from the 5d excited state to the 4f ground state and a resultant red-shift of the emission. The estimated Stokes shifts and CIE chromaticity coordinates of $Sr_8ZnSc(PO_4)_7$:xEu^{2+} (x = 0.001−0.05 mol) are 8966−9735 cm^{-1} and (0.3835, 0.5074) to (0.4221, 0.5012), respectively. The broad asymmetric yellow-emitting band of $Sr_8ZnSc(PO_4)_7$:xEu^{2+} was attributed to the $4f^65d^1 \rightarrow 4f^7$ electronic dipole allowed transitions of Eu^{2+} ions occupying different cation ions and coordination environments in the $Sr_8ZnSc(PO_4)_7$ host.

dx.doi.org/10.1021/am302014e | ACS Appl. Mater. Interfaces 2012, 4, 6661−6668

Table 2. Excitation and Emission Bands, Stokes Shift, Crystal Field Splitting, Normalized PL Intensity, and the CIE Coordinates of $Sr_8ZnSc(PO_4)_7:xEu^{2+}$ (x = 0.001−0.05 mol) Phosphors

Eu^{2+} conc.	λ_{ex} range (nm)	fwhm of λ_{ex} (nm)	λ_{em} (nm)	Stokes shift (cm^{-1})	crystal field splitting (cm^{-1})	relative PL intensity (%)	CIE (x, y)
0.001	240−450	132	547	8966	20181	75.5	(0.3835, 0.5074)
0.003	240−460	137	550	9066	20188	80.5	(0.3892, 0.5066)
0.005	240−470	140	552	9132	20319	85.5	(0.3897, 0.5061)
0.010	240−480	144	554	9197	20448	93.7	(0.3927, 0.5054)
0.020	240−490	151	562	9454	20786	100.0	(0.4108, 0.5042)
0.030	240−500	154	569	9673	20991	90.8	(0.4195, 0.5030)
0.040	240−500	156	570	9704	20822	85.6	(0.4201, 0.5022)
0.050	240−500	156	571	9735	20983	65.0	(0.4221, 0.5012)

According to the report of Van Uitert,[20] the possible crystallographic site can be investigated theoretically by the following equation[21]

$$E = Q\left[1 - \left(\frac{V}{4}\right)^{1/V} 10^{-nE_a r/80}\right] \quad (1)$$

where E represents the position of the d-band edge in energy for the rare-earth ion (cm^{-1}), Q is the position in energy for the lower d-band edge for the free ion (34 000 cm^{-1} for Eu^{2+}); V is the valence of the activator (Eu^{2+}) ion (V = 2), n is the number of anions in the immediate shell about the Eu^{2+} ion, r is the radius of the host cation replaced by the Eu^{2+} ion (in Å), E_a is the electron affinity of the atoms that form anions (in eV). For PO_4^{3-} phosphor, the value of E_a is approximately 2.19 eV.[22] Table 3 show the experimental and calculated emission

Table 3. Experimental and Calculated Emission Wavelengths of Eu^{2+} Ions Occupying Different Cation Ions and Coordination Environments in the $Sr_8ZnSc(PO_4)_7$ Host

n	r (Å)	E_{calcd} (cm^{-1})	λ_{calcd} (nm)	λ_{exp} (nm)
8	r_{Sr}/1.26	21264	470	510 and 547−571
9	r_{Sr}/1.31	22566	443	
8	R_{Zn}/0.9	18729	534	
6	R_{Sc}/0.9	15862	630	

wavelengths of Eu^{2+} ions occupying different cation ions and coordination environments in the $Sr_8ZnSc(PO_4)_7$ host. The result indicate that the experimental values agree well with the calculated values and the broad asymmetric yellow-emitting band is due to Eu^{2+} ions occupying eight-coordinated Sr^{2+} and Zn^{2+}, and six-coordinated Sc^{3+} site.

Figure 4 illustrates the concentration dependence of the emission intensity of $Sr_8ZnSc(PO_4)_7:xEu^{2+}$ (x = 0.001−0.05 mol) under 400 nm excitation. The optimal doping concentration for the PL intensity was 0.02 mol under 400 nm excitation, and the emission efficiency of $Sr_8ZnSc(PO_4)_7$:0.02Eu^{2+} phosphor compared with that of the commercial YAG:Ce^{3+} (excited at 460 nm) phosphor is calculated to be 32.5%. The lower luminescence of $Sr_8ZnSc(PO_4)_7$:0.02Eu^{2+} could be further enhanced by process optimization. The emission intensity increased with increasing x when x < 0.02 and the Eu^{2+} doped content exceeded 0.02 mol, concentration quenching was observed, and the emission intensity decreased with increasing Eu^{2+} content. According to the percolation model, concentration quenching of the compound can occur by two mechanisms:[23] (1) interactions between the Eu^{2+} ions, which result in energy reabsorption among neighboring Eu^{2+} ions in the rare-earth sublattice; (2)

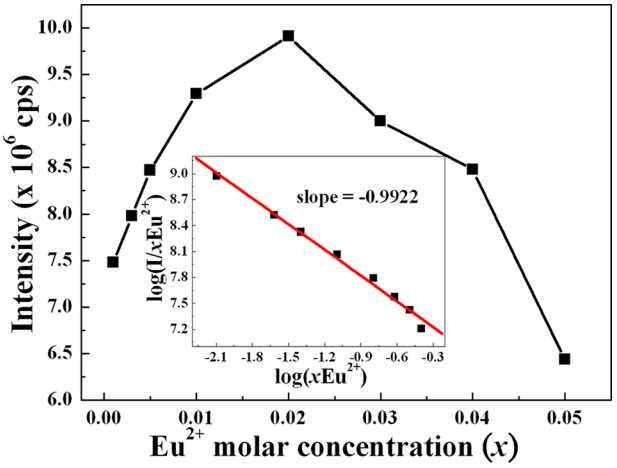

Figure 4. Concentration dependence of emission intensity of $Sr_8ZnSc(PO_4)_7:xEu^{2+}$ (x = 0.001−0.05 mol) under 400 nm excitation. The inset illustrates the I/x dependence on x on a logarithmic scale.

energy transfer from a percolating cluster of Eu^{2+} ions to the killer centers.

Nonradiative energy transfer between the Eu^{2+} ions may take place via an exchange interaction or an electric multipolar interaction. The exchange interaction requires a large direct or indirect overlap of the wave functions of the donor and acceptor, and this mechanism is responsible for energy transfer in the case of forbidden transitions. The critical distance for the exchange interaction is approximately 5 Å.[24] This indicates that the mechanism of exchange interaction plays no role in energy transfer between Eu^{2+} ions in the $Sr_8ZnSc(PO_4)_7:xEu^{2+}$ phosphor. However, energy transfer between the Eu^{2+} ions in the $Sr_8ZnSc(PO_4)_7:xEu^{2+}$ phosphor was attributed to nonradiative electric multipolar interaction. The mechanism of interaction between the Eu^{2+} ions can be expressed by the following equation[25]

$$\frac{I}{x} = \frac{k}{1 + \beta(x)^{\theta/3}} \quad (2)$$

where k and β are constants for each interaction for a given host lattice, χ is the activator concentration; According to the research result of Van Uitert, θ = 3 for the energy transfer among the nearest-neighbor ions, as θ = 6, 8, 10 corresponds to dipole−dipole, dipole−quadrupole, quadrupole−quadrupole interactions, respectively. The inset of Figure 4 illustrates the I/x dependence on x on a logarithmic scale. $\log(I/x Eu^{2+})$ showed a relatively linear dependence on $\log(x Eu^{2+})$, and the slope was determined to be −0.9922. The value of θ was found to be approximately 3. This result indicated that the energy

dx.doi.org/10.1021/am302014e | ACS Appl. Mater. Interfaces 2012, 4, 6661−6668

transfer among the nearest-neighbor ions and the quenching was proportional to the Eu^{2+} ions concentration in the SZSP:xEu^{2+} phosphor.[26] The critical distance R_c was estimated by Blasse using the following equation[27]

$$R_c \approx 2\left[\frac{3V}{4\pi x_c N}\right]^{1/3} \quad (3)$$

where V is the volume of the unit cell, and N is the number of host cations in the unit cell. The values of V and N are 2600.74 Å^3 and 4. The Eu^{2+}−Eu^{2+} distance R_{Eu-Eu} in SZSP:xEu^{2+} was determined to be 53.74, 37.26, 31.43, 24.94, 19.80, 17.30, 15.71, and 14.59 Å for x = 0.001, 0.003, 0.005, 0.01, 0.02, 0.03, 0.04, and 0.05, respectively. The aforementioned result indicated that with an increase in the doped Eu^{2+} molar concentration, R_c decreased and the crystal-field splitting of the 5d bands of the Eu^{2+} ions increased, leading to a continuous increase in the redshift with the doped Eu^{2+} concentration (Figure 3b and Table 2).The critical concentration (x_c) of Eu^{2+} in the SZSP host was found to be 0.02 mol. Therefore, the R_c value for energy transfer was calculated to be 19.80 Å.

3.3. Reflectance Spectra Properties. The diffuse reflectance spectra of $Sr_8ZnSc(PO_4)_7$ and $Sr_8ZnSc(PO_4)_7$:0.02Eu^{2+} and the PL/PLE spectra of $Sr_8ZnSc(PO_4)_7$:0.02Eu^{2+} are shown in Figure 5. The SZSP host

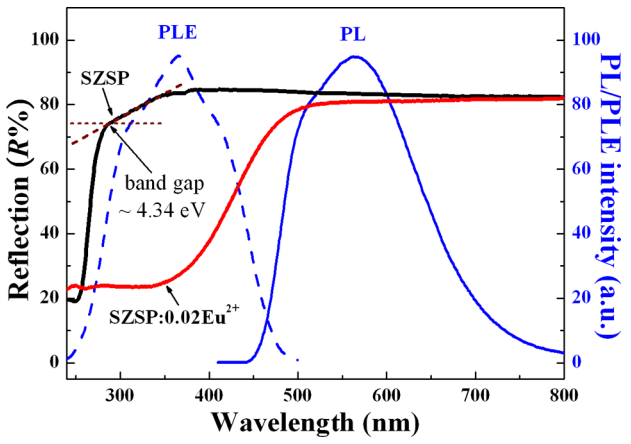

Figure 5. Diffuse reflectance spectra of $Sr_8ZnSc(PO_4)_7$ (black line) and $Sr_8ZnSc(PO_4)_7$:0.02Eu^{2+} (red line), and PL/PLE spectra of $Sr_8ZnSc(PO_4)_7$:0.02Eu^{2+} phosphor.

material showed energy absorption in the ≤350 nm region,[28] and the band gap was estimated to be about 4.34 eV (34965 cm^{-1}). As Eu^{2+} ions were doped into the SZSP host, the reflection spectra of the host became different from that of SZSP:0.02Eu^{2+}: a strong broad absorption, assigned to the 4f^7 → 4f^{6}5d^1 absorption of the Eu^{2+} ions, was observed in the 240−500 nm NUV range for SZSP:0.02Eu^{2+}. The broad absorption from 240 to 450 nm for the SZSP:0.02Eu^{2+} phosphor matched well with the excitation spectra. The as-synthesized SZSP:0.02Eu^{2+} phosphor exhibited very broad excitation bands (PLE spectra) from 240 to 500 nm, indicating efficient excitation of the phosphor by the NUV LED chips (380−420 nm) for applications in white NUV LEDs. The emission spectra showed a strong, broad yellow emission band in the range 450−800 nm, centered at 511 and 564 nm, typically attributed to the 4f^{6}5d^1 → 4f^7 electronic-dipole-allowed transitions of Eu^{2+} ions. The broad asymmetric emission band for SMGP:Eu^{2+} was attributed to the transition of Eu^{2+} occupying the five crystallographically distinct Sr^{2+} sites in the SZSP host.[29]

3.4. EL Spectrum of White-Light LED Lamp. To demonstrate the potential application of $Sr_8ZnSc(PO_4)_7$:xEu^{2+} phosphors, white LED lamps were fabricated using a 400 nm NUV chip combined with a blend of blue-emitting $BaMgAl_{10}O_{17}$:Eu^{2+} (BAM:Eu^{2+}) and yellow-emitting $Sr_8ZnSc(PO_4)_7$:xEu^{2+} phosphors driven by 350 mA current. Figure 6

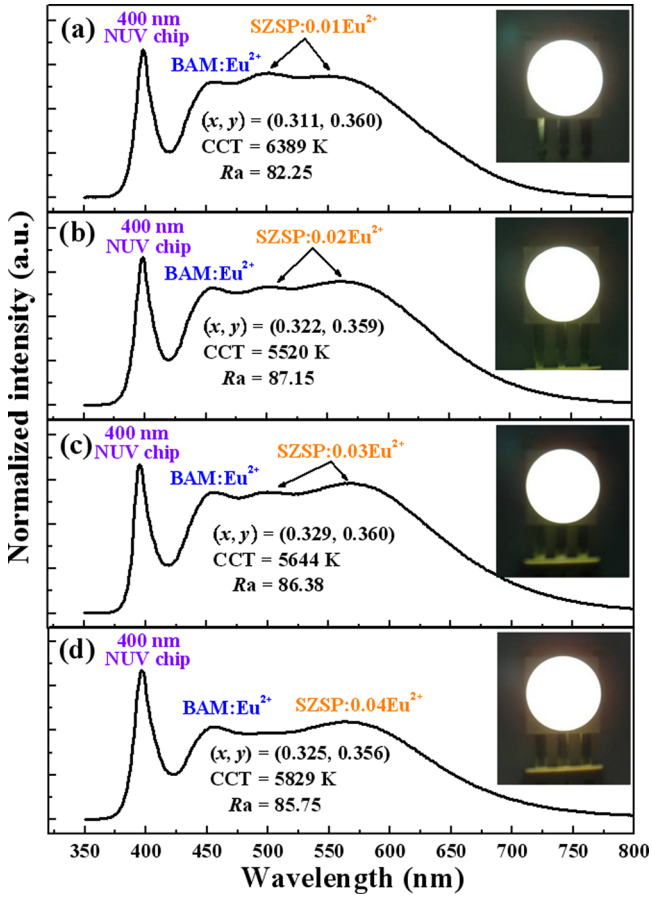

Figure 6. Electroluminescent spectra of white-LED lamps fabricated using a 400 nm NUV chip combined with a blend of blue-emitting $BaMgAl_{10}O_{17}$:Eu^{2+} and yellow-emitting (a) $Sr_8ZnSc(PO_4)_7$:0.01Eu^{2+}, (b) $Sr_8ZnSc(PO_4)_7$:0.02Eu^{2+}, (c) $Sr_8ZnSc(PO_4)_7$:0.03Eu^{2+}, (d) $Sr_8ZnSc(PO_4)_7$:0.04Eu^{2+} phosphors. Insets show the photograph of the LED lamp package driven by 350 mA current.

shows the electroluminescence (EL) spectra of the lamps. Four emission bands could be clearly seen in Figures 6a−d: 400 nm, attributed to the NUV chip; 454 nm, attributed to BAM:Eu^{2+}; and 511−571 nm, attributed to the SZSP:xEu^{2+} phosphor. With increasing Eu^{2+} doped concentration, the CIE chromaticity coordinates (x, y) of the white LEDs were measured as (0.311, 0.360), (0.322, 0.359), (0.329, 0.360) eventually to (0.325, 0.356) for SZSP:xEu^{2+} phosphors with x = 0.01, 0.02, 0.03, and 0.04. The color rendering index (CRI) increased when the Eu^{2+}-doped concentration was less than 0.02 mol, and hence, the optimal Eu^{2+} ion concentration was identified to be 0.02 mol (CRI, Ra = 87.15, Figure 6b). However, the correlated color temperature (CCT) decreased as the Eu^{2+} concentration increased, reaching a maximum at x = 0.02 mol (5520 K), and then increased from 5520 K (Figure 6b) to 5829 K (Figure 6d). The luminous efficacy of 400 nm NUV chip combined with a

dx.doi.org/10.1021/am302014e | ACS Appl. Mater. Interfaces 2012, 4, 6661−6668

blend of BAM:Eu^{2+} and SZSP:xEu^{2+} white LED were measured to be 15.3, 13.2, 10.9, and 9.6 lm/W for Figure 6a to Figure 6d. The lower values of luminous efficacy of the fabricated white LEDs were due to poor chip and quantum efficiencies. The insets of Figure 6a–d show the photographs of a white LED lamp package driven by 350 mA current.

Figure 7a shows the EL spectrum of white LEDs composed of a 400 nm NUV chip and a phosphor blend of

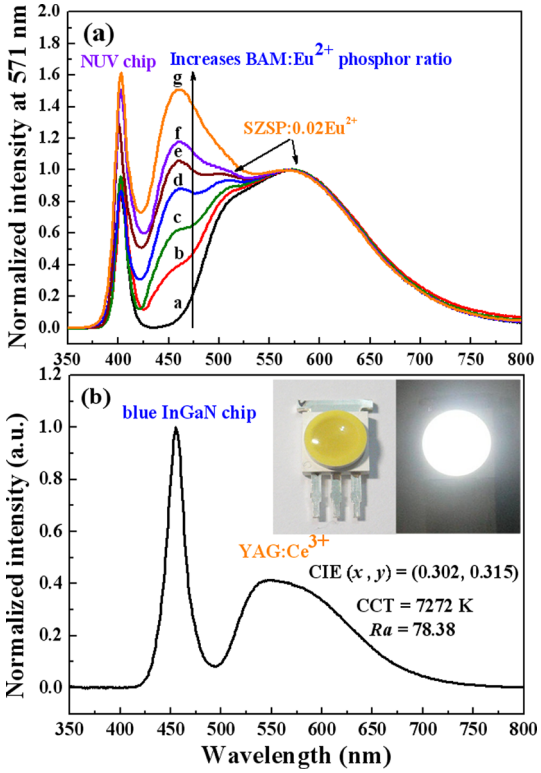

Figure 7. EL spectrum of white LEDs composed of (a) 400 nm NUV chip and a phosphor blend of $BaMgAl_{10}O_{17}:Eu^{2+}$ and $Sr_8ZnSc(PO_4)_7:0.02Eu^{2+}$ in various mixing ratios; (b) InGaN chip pumped with YAG:Ce^{3+} phosphor, driven by 350 mA current.

$BaMgAl_{10}O_{17}:Eu^{2+}$ and $Sr_8ZnSc(PO_4)_7:0.02Eu^{2+}$ in various mixing ratios. The EL spectrum of the white LEDs shows four emission bands at 400, 454, 501, and 562 nm, which are due to the NUV chip, BAM:Eu^{2+}, and SZSP:0.02Eu^{2+} phosphors, respectively. The EL spectrum of BAM:Eu^{2+} at 454 nm increases with increasing BAM:Eu^{2+} weight ratio. When the BAM:Eu^{2+} weight ratio is increased, the CCT continuously increases from 3868 to 7937 K, while *Ra* gradually increases from 66.38 to a maximum of 92.88, as shown in Table 4 (point g in Figure 7a). The eight CRIs and average *Ra* values of the white LEDs driven by 350 mA current are listed in Table S2 in the Supporting Information. On the other hand, *Ra* and the CIE color coordinates of the white LED with the blue InGaN chip pumped to the YAG:Ce^{3+} phosphor, whose spectrum is shown in Figure 7b, are 78.38 and (0.302, 0.315), respectively, at a CCT of 7272 K. The white NUV LEDs fabricated in this study show high *Ra* values and low CCT values. Therefore, the results indicate that the BAM:Eu^{2+}/SZSP:0.02Eu^{2+} blends display suitable colors and tunable CCT and high *Ra* values for application in white NUV LEDs. Figure 8 shows the electroluminescence spectra of the fabricated white LED under various currents (150–750 mA). The inset of

Table 4. CIE Chromaticity Coordinates, CCT, and *Ra* of White LEDs Having a Phosphor Blend of BAM:Eu^{2+} and SZSP:0.02Eu^{2+} with 400 nm NUV Chip Driven by 350 mA Current

	CIE coordinates			
white-light LEDs CIE site	*x*	*y*	CCT (K)	*Ra*
a	0.421	0.497	3868	66.38
b	0.381	0.435	4325	79.38
c	0.360	0.405	4721	82.13
d	0.336	0.372	5370	85.75
e	0.322	0.349	5956	88.88
f	0.314	0.336	6395	90.63
g	0.294	0.310	7937	92.88
w	0.302	0.315	7272	78.38

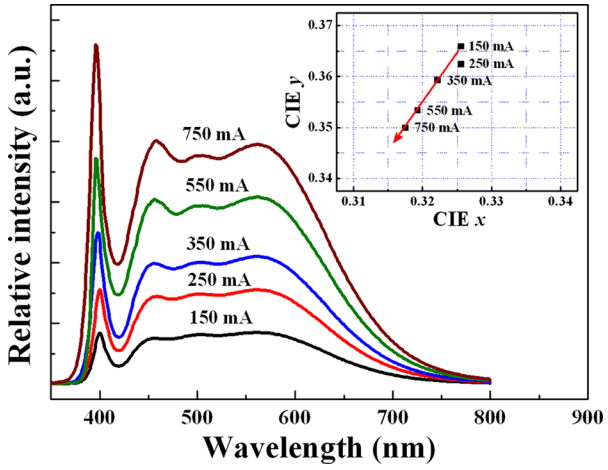

Figure 8. Electroluminescence spectra of the fabricated white LED under various currents (150–750 mA). The inset displays the variation in CIE chromaticity coordinates of white LED operated under different currents.

Figure 8 displays the variation of CIE chromaticity coordinates of white LED operated under different currents. With increasing the current from 150 mA to 750 mA, the CIE chromaticity coordinates blue-shift slightly tuned from (0.3256, 0.3659) at 150 mA to (0.3222, 0.3593) at 350 mA and eventually to (0.3175, 0.3499) at 750 mA with correlated color temperature 5481, 5520, and 5903 K. The color rendering index *Ra* of the fabricated LED was found to increase from 85.1 to 87.9 with increasing the forward-bias current, as shown in Table S3 in the Supporting Information. The results demonstrated the excellent color stability of $Sr_8ZnSc(PO_4)_7:Eu^{2+}$ phosphors with different driving currents.

Figure 9 shows the CIE chromaticity diagram of white LEDs with various $BaMgAl_{10}O_{17}:Eu^{2+}$ and $Sr_8ZnSc(PO_4)_7:0.02Eu^{2+}$ mixing ratios. By weight ratio tuning, the outputs of the BAM:Eu^{2+} and SZSP:0.02Eu^{2+} phosphors were found to systematically emit hues and chromaticity coordinates (*x*, *y*) of whitet LEDs from yellow-light (point a, (0.421, 0.497)) through warm-white (point c, (0.360, 0.405)) and then to white-light (point f, (0.314, 0.336)) region with increasing BAM:Eu^{2+} weight ratio. The inset shows the photograph of the LED package driven by 350 mA current. For comparison, a blue InGaN chip pumped with YAG:Ce^{3+} phosphor was considered, and this system was found to emit white light with CIE chromaticity coordinates of (0.302, 0.315). The white NUV LEDs fabricated in this study (point e) showed higher *Ra*

dx.doi.org/10.1021/am302014e | ACS Appl. Mater. Interfaces 2012, 4, 6661–6668

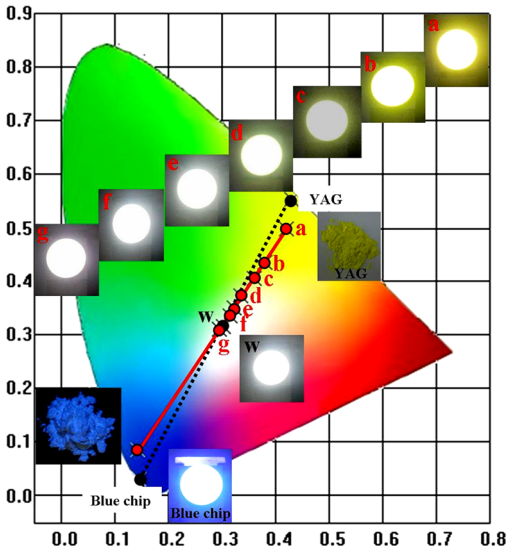

Figure 9. CIE chromaticity diagram of white LEDs with $BaMgAl_{10}O_{17}:Eu^{2+}$ and $Sr_8ZnSc(PO_4)_7:0.02Eu^{2+}$ phosphors in various mixing ratios. Inset shows the photograph of the LED package driven by 350 mA current.

values (88.88 for SZSP:0.02Eu^{2+}, 78.38 for YAG:Ce^{3+}) and lower CCT values (5956 K for SZSP:0.02Eu^{2+}, 7272 K for YAG:Ce^{3+}). The results obtained for the LED package demonstrated that SZSP:0.02Eu^{2+} has potential applications in the white NUV LEDs with excellent *Ra*.

4. CONCLUSIONS

In summary, a novel Eu^{2+}-activated $Sr_8ZnSc(PO_4)_7$ yellow-emitting phosphor has been synthesized and evaluated for use in white NUV LEDs. The excitation and reflectance spectra of this phosphor show strong broad absorption in the 240−500 nm region, which matches well with that in the case of NUV chips; the emission intensity of the optimized $Sr_8ZnSc(PO_4)_7:Eu^{2+}$ is 0.02 mol under 400 nm excitation. The emission band shows a redshift (from 547 to 571 nm) with increasing Eu^{2+} concentration, mainly because of the change in the crystal-field splitting of Eu^{2+}. The emission wavelength, Stokes shift, crystal-field splitting, and CIE chromaticity coordinates of the $Sr_8ZnSc(PO_4)_7$ (x = 0.001−0.05 mol) phosphors are estimated to be in the range 547−571 nm, 8966−9735 cm^{-1}, 20181−20983 cm^{-1}, and (0.3835, 0.5074) to (0.4221, 0.5012), respectively, depending on the Eu^{2+} molar concentration. Moreover, white NUV LEDs are fabricated by integrating a 400 nm NUV chip and a mixture of yellow-emitting $Sr_8ZnSc(PO_4)_7:0.02Eu^{2+}$ and blue-emitting BAM:Eu^{2+} phosphors into a single package. Under 350 mA forward-bias current, the package shows a high *Ra* between 79.38 and 92.88, CCT between 4325 and 7937 K, and tuned CIE chromaticity coordinates ranging from (0.381, 0.435) to (0.294, 0.310) when the yellow-to-blue-phosphor weight ratio is changed. These results demonstrate that $Sr_8ZnSc(PO_4)_7:xEu^{2+}$ phosphors have considerable potential for use in NUV chips as compared to that incorporating YAG:Ce^{3+} and pumped by blue LED chips [CIE = (0.302, 0.315), CCT = 7272 K, *Ra* = 78.38]. Therefore, our novel yellow-emitting $Sr_8ZnSc(PO_4)_7:Eu^{2+}$ phosphor can serve as the key material for phosphor-converted white NUV LEDs.

■ ASSOCIATED CONTENT

Ⓢ Supporting Information

Atomic positions and lattice parameters for $Sr_8ZnSc(PO_4)_7:0.05Eu^{2+}$ phosphors; eight CRIs and *Ra* values of white LEDs having a phosphor blend of BAM:Eu^{2+} and SZSP:0.02Eu^{2+} with 400 nm NUV chip driven by 350 mA current; CIE chromaticity coordinates, CCT, *Ra* of as-fabricated white-LED under various currents (150−750 mA). This material is available free of charge via the Internet at http://pubs.acs.org.

■ AUTHOR INFORMATION

Corresponding Author

*Tel: +886-3-5732438. E-mail: Chien-Hao@itri.org.tw (C.-H.H.); tmchen@mail.nctu.edu.tw (T.-M.C.).

Notes

The authors declare no competing financial interest.

■ ACKNOWLEDGMENTS

This research were supported by Industrial Technology Research Institute under Contract B301AR4850 (C.H.H.) and in part by National Science Council of Taiwan under Contract NSC101-2113-M-009-021-MY3 (T.M.C.).

■ REFERENCES

(1) Kim, J. S.; Jeon, P. E.; Choi, J. C.; Park, H. L.; Mho, S. I.; Kim, G. C. *Appl. Phys. Lett.* **2004**, *84*, 2931−2933.
(2) Im, W. B.; Kim, Y. I.; Fellows, N. N.; Masui, H.; Hirata, G. A.; Den, S. P.; Seshadri, B. R. *Appl. Phys. Lett.* **2008**, *93*, 091905.
(3) Nishida, T.; Ban, T.; Kobayashi, N. *Appl. Phys. Lett.* **2003**, *82*, 3817−3819.
(4) Muthu, S.; Schuurmans, F. J. P.; Pashley, M. D. *IEEE. J. Sel. Top. Quantum Electron.* **2002**, *8*, 333−338.
(5) Lee, S.; Seo, S. Y. *J. Electrochem. Soc.* **2002**, *149*, J85−j88.
(6) Huang, C. H.; Chen, T. M. *J. Phys. Chem. C* **2011**, *115*, 2349−2355.
(7) Huang, C. H.; Wu, P. J.; Lee, J. F.; Chen, T. M. *J. Mater. Chem.* **2011**, *21*, 10489−10495.
(8) Jang, H. S.; Won, Y. H.; Jeon, D. Y. *Appl. Phys. B: Laser Opt.* **2009**, *95*, 715−720.
(9) Xia, Z.; Zhuang, J.; Liao, L.; Liu, H.; Luo, Y.; Du, P. *J. Electrochem. Soc.* **2011**, *158*, J359−J362.
(10) Zhang, X.; Fei, L.; Shi, J.; Gong, M. *Physica B* **2011**, *406*, 2616−2620.
(11) Wu, Z.; Gong, M.; Shi, J.; Wang, G.; Su, Q. *Chem. Lett.* **2007**, *36*, 410−411.
(12) Jang, H. S.; Kim, H. Y.; Kim, Y. S.; Lee, H. M.; Jeon, D. Y. *Opt. Express* **2012**, *20*, 2761−2771.
(13) Song, W. S.; Kim, Y. S.; Yang, H. *Mater. Chem. Phys.* **2009**, *117*, 500−503.
(14) Jang, H. S.; Jeon, D. Y. *Opt. Lett.* **2007**, *32*, 3444−3446.
(15) Wu, Y. C.; Chen, T. M.; Chiu, C. H.; Mo, C. N. *J. Electrochem. Soc.* **2010**, *157*, J342−J346.
(16) Larson, A. C.; Von Dreele, R. B. *Generalized Structure Analysis System (GSAS), Los Alamos National Laboratory Report LAUR 86-748*; Los Alamos National Laboratory: Los Alamos, NM, 1994.
(17) Belik, A. A.; Izumi, F.; Ikeda, T.; Okui, M.; Malakho, A. P.; Morozov, V. A.; Lazoryak, B. I. *J. Solid State Chem.* **2002**, *168*, 237−244.
(18) Huang, C. H.; Luo, L.; Chen, T. M. *J. Electrochem. Soc.* **2011**, *158*, J341−J344.
(19) Chiu, Y. C.; Huang, C. H.; Lee, T. J.; Liu, W. R.; Yeh, Y. T.; Jang, S. M.; Liu, R. S. *Opt. Express* **2011**, *19*, A331−A339.
(20) Van Uitert, L. G. *J. Lumin.* **1984**, *29*, 1−9.
(21) Xia, Z.; Liu, R. S.; Huang, K. W.; Drozd, V. *J. Mater. Chem.* **2012**, *22*, 15183−15189.

(22) Li, P. L.; Yang, Z. P.; Wang, Z. J.; Guo, Q. L. *Chin. Phys. B* **2008**, *17*, 1135−1138.
(23) Kuo, T. W.; Huang, C. H.; Chen, T. M. *Opt. Express* **2010**, *18*, A231−A236.
(24) Dexter, D. L. *J. Chem. Phys.* **1953**, *21*, 836−850.
(25) Vanuiter, L. G. *J. Electrochem. Soc.* **1967**, *114*, 1048−1053.
(26) Xia, Z.; Liu, J.; Li, Q.; Sun, J. *Electrochem. Solid-State Lett.* **2007**, *1*, J4−J8.
(27) Blasse, G. *Philips Res. Rep.* **1969**, *24*, 131−144.
(28) Huang, C. H.; Chen, T. M. *Inorg. Chem.* **2011**, *50*, 5725−5730.
(29) Zhang, X.; Chen, H.; Ding, W.; Wu, H.; Kim, J. *J. Am. Ceram. Soc.* **2009**, *92*, 429−432.